ISSN 1070-3284, Russian Journal of Coordination Chemistry, 2019, Vol. 45, No. 6, pp. 402–410. © Pleiades Publishing, Ltd., 2019.
Russian Text © The Author(s), 2019, published in Koordinatsionnaya Khimiya, 2019, Vol. 45, No. 6, pp. 341–349.

Spin State of the Iron(II) and Cobalt(II) 2,6-Di(5-Amino-1*H*-Pyrazol-3-yl)pyridine Complexes in Solution and in Crystal

A. A. Pavlov[a], I. A. Nikovskii[a], A. V. Polezhaev[a, b], D. Yu. Aleshin[a, c], E. K. Melnikova[a, d], Ya. A. Pankratova[d], and Yu. V. Nelyubina[a, e, *]

[a] *Nesmeyanov Institute of Organoelement Compounds, Russian Academy of Sciences, 119991 Russia*
[b] *Bauman State Technical University, Moscow, 107005 Russia*
[c] *Mendeleev University of Chemical Technology, Moscow, 125190 Russia*
[d] *Moscow State University, Moscow, 119899 Russia*
[e] *Kurnakov Institute of General and Inorganic Chemistry, Russian Academy of Sciences, Moscow, 119991 Russia*
**e-mail: unelya@ineos.ac.ru*

Received November 13, 2018; revised January 17, 2019; accepted January 24, 2019

Abstract—The cobalt(II) and iron(II) complexes with 2,6-di(5-amino-1*H*-pyrazol-3-yl)pyridine (L), $CoL_2(ClO_4)_2$ (**I**) and $FeL_2(ClO_4)_2$ (**II**), are synthesized by the template reaction, isolated in the individual form, and characterized by elemental analysis, NMR spectroscopy, and thermogravimetry. The structures of complexes **I** and **II** (including the iron(II) complex obtained as two new solvate forms ($FeL_2(ClO_4)_2 \cdot 2(C_2H_5)_2O \cdot H_3CN$ (**IIa**) and $FeL_2(ClO_4)_2 \cdot (C_2H_5)_2O \cdot CH_3CN \cdot 0.75H_2O$ (**IIb**)) are confirmed by X-ray diffraction analysis. The data obtained in the crystal (by the X-ray diffraction method) and in solutions (using the proposed approach to an analysis of paramagnetic shifts in ^{1}H NMR spectra) indicate that the metal ion in the complexes exists in the high-spin state ($S = 3/2$ for Co(II) and $S = 2$ for Fe(II)) and undergoes no temperature-induced spin transition in a range of 120–300 K.

Keywords: transition metal complexes, spin state, spin transition, NMR spectroscopy

DOI: 10.1134/S1070328419060046

INTRODUCTION

Molecular systems characterized by bistability, i.e., capable of existing in two different electron states under certain conditions [1], form a basis for advanced concepts of superdense information storage and quantum computers [2], switches, sensors, and other molecular devices and materials [3–5]. Typical examples of these bistable systems are transition metal complexes with the d^4–d^7-electronic configuration (mainly of iron(II), iron(III), and cobalt(II) [6]) capable of transiting from one spin state to another when an appropriate external stimulus (temperature, pressure, light, magnetic and electric fields, etc.) is applied [6, 7]. The possibility of the spin transition to occur is determined by the local environment of the metal ion, while its parameters depend, to a significant extent, on interactions between molecules of the complex due to which a sharp spin transition with hysteresis is possible in the crystalline sample [6]. Even slight changes at the periphery of the molecule can result in a change in the populations of the spin states [8, 9]. In some cases, the shift of the spin equilibrium results from different phase states of the studied compound (single crystal, polycrystalline powder, or solution) [10], differences in the crystal packing (different polymorphous modifications [11]), and even solvent effects [11–13].

The compounds that undergo the temperature-induced spin transition, the iron(II) 2,6-di(pyrazol-1-yl)pyridine complexes [14, 15], are most studied due to their synthetic accessibility and the possibility to control the spin state of the metal ion by choosing an appropriate substituent [16]. To find similar relationships "structure–property" for the complexes with isomeric ligands, 2,6-di(1*H*-pyrazol-3-yl)pyridines, which have equally wide possibilities of functionalization [17] but are more prone to the influence of the environment on the spin state of the metal ion [5], more new derivatives need to be obtained [17] and their properties studied in various phase states and in the form of diverse polymorphic and solvatomorphic modifications.

The temperature-induced spin transition in the polycrystalline sample was observed for the iron(II) complex with 2,6-di(5-amino-1*H*-pyrazol-3-yl)pyridine (L) [18] obtained as dihydrate $FeL_2(ClO_4)_2 \cdot 2H_2O$, with most of the sample remained in the high-spin state.

In this work, we synthesized the earlier unknown complex $CoL_2(ClO_4)_2$ (**I**) and complex $FeL_2(ClO_4)_2$ (**II**) as two new solvate forms simultaneously precipitating during crystallization (Scheme 1) and analyzed their spin states in solutions and in the crystal.

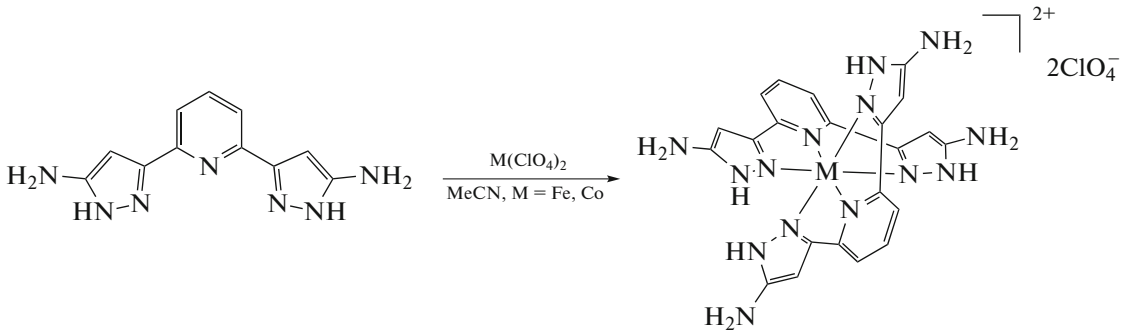

Scheme 1.

EXPERIMENTAL

All procedures on the synthesis of the complexes were carried out in air using commercially available organic solvents and reagents. Cobalt salt $Co(ClO_4)_2 \cdot 6H_2O$ [19] and ligand L [8, 20, 21] were synthesized using earlier described procedures. Analyses to the contents of carbon, nitrogen, and hydrogen were carried out on a CarloErba microanalyzer (model 1106). The thermogravimetric analyses of complexes **I** and **II** were conducted on a NetzchTG 209 F1 Libra instrument in a range of 20–500°C with the heating rate 7 K/min in argon.

Synthesis of $CoL_2(ClO_4)_2$ (I). Weighed samples of $Co(ClO_4)_2 \cdot 6H_2O$ (22.7 mg, 0.0622 mmol) and L (30 mg, 0.124 mmol) were dissolved or suspended in anhydrous acetonitrile (10 mL) to form a dark brown solution. The reaction mixture was stirred for 1 h at room temperature, and precipitation was observed. The obtained precipitate was separated and purified by recrystallization from an acetonitrile–diethyl ether (1 : 1) system. The yield of the product was 29.5 mg (64%).

For $C_{22}H_{24}N_{14}O_9Cl_2Co$

Anal. calcd., %	C, 34.84	H, 3.19	N, 25.86
Found, %	C, 34.72	H, 3.37	N, 25.58

^{1}H NMR (CD_3CN), δ, ppm: 1.38 (br.s, 2H, 4-Py), 21.29 (br.s, 8H, NH_2), 28.52 (br.s, 4H, 3-Py), 54.58 (br.s, 4H, 4-Pz), 82.34 (br.s, 4H, NH).

Synthesis of $FeL_2(ClO_4)_2$ (II). Weighed samples of $Fe(ClO_4)_2$ (15.8 mg, 0.0622 mmol) and L (30 mg, 0.124 mmol) were dissolved or suspended in anhydrous acetonitrile (10 mL) to form a dark brown solution. The reaction mixture was stirred for 1 h at room temperature, and a precipitate of the target product was formed. The obtained precipitate was separated and purified by recrystallization from an acetonitrile–diethyl ether (1 : 1) system. The yield of the product was 25.2 mg (55%).

For $C_{22}H_{22}N_{14}O_8Cl_2Fe$

Anal. calcd., %	C, 35.84	H, 3.01	N, 26.60
Found, %	C, 34.57	H, 2.81	N, 26.51

^{1}H NMR (CD_3CN), δ, ppm: 9.7 (br.s, 8H, NH_2), 27.64 (br.s, 4H, NH), 30.07 (br.s, 2H, 4-Py), 52.11 (br.s, 4H, 3-Py), 60.71 (br.s, 4H, 4-Pz).

X-ray diffraction analyses (XRD) of the single crystals of complexes **I** and **II** (as two solvatomorphs **IIa** and **IIb** obtained by slow evaporation in air from an acetonitrile–diethyl ether (1 : 1) mixture of solvents) were carried out on a Bruker APEX2 DUO CCD diffractometer (MoK_α radiation, graphite monochromator, ω scan mode) at 120 K. The structures were solved by a direct method and refined by least squares in the anisotropic full-matrix approximation for F^2_{hkl}. The hydrogen atoms of the NH and NH_2 groups and of the solvate water molecules (presumably "captured" from air during crystallization) were located from the difference Fourier syntheses and refined in the isotropic approximation by the riding model. The main crystallographic data and refinement parameters are presented in Table 1. All calculations were performed using the SHELXTL PLUS program package [22].

The structural data for compounds **I**, **IIa**, and **IIb** were deposited with the Cambridge Crystallographic Data Centre (CIF files CCDC nos. 1876396, 1876397, and 1876398, respectively; http://www.ccdc.cam.ac.uk/).

The ^{1}H NMR spectra of complexes **I** and **II** were recorded in CD_3CN on a Bruker Avance 600 spectrometer (600.22 MHz). Chemical shifts (δ, ppm) in the spectra were determined relative to the residual

Table 1. Selected crystallographic data and structure refinement parameters for compounds **I**, **IIa**, and **IIb**

Parameter	Value		
	I	**IIa**	**IIb**
Empirical formula	$C_{28}H_{36.12}N_{15}O_{9.56}Cl_2Co$	$C_{32}H_{45}N_{15}O_{10}Cl_2Fe$	$C_{28}H_{36.5}N_{15}O_{9.75}Cl_2Fe$
FW	865.54	926.58	865.97
T, K	120	120	120
Crystal system	Monoclinic	Orthorhombic	Monoclinic
Space group	$P2_1/n$	*Pbcn*	$P2_1/n$
Z	4	4	4
a, Å	15.1212(9)	14.226(1)	14.941(2)
b, Å	14.4842(9)	23.453(2)	14.729(2)
c, Å	18.134(1)	12.787(1)	18.031(2)
β, deg	111.9950(10)	90	111.193(2)
V, Å^3	3682.6(4)	4266.3(6)	3699.8(6)
ρ_{calcd}, g cm^{-3}	1.561	1.443	1.555
μ, cm^{-1}	6.86	5.50	6.27
F(000)	1786	1928	1790
$2\theta_{max}$, deg	52	58	52
Number of measured reflections	71353	66925	35867
Number of independent reflections	7245	5677	7269
Number of reflections with $I > 2\sigma(I)$	6063	4441	5408
Number of refined parameters	543	276	527
R_1	0.0579	0.0380	0.0636
wR_2	0.1530	0.1048	0.1775
GOOF	1.076	1.049	1.019
Residual electron density ($\Delta\rho_{min}/\Delta\rho_{max}$), *e* Å^{-3}	−0.722/1.631	−0.366/0.516	−0.939/1.894

signal of the solvent (^{1}H 1.94 ppm). The spectra were recorded using the following parameters: spectral range 200 ppm, detection time 0.5 s, relaxation delay 0.5 s, pulse duration 6.5 μs, and number of scans 128. To increase the signal to noise ratio, the obtained free induction decays were processed using exponential weighing with the coefficient lower than 3 Hz.

The quantum chemical calculations for complexes **I** and **II** were performed using the ORCA program package (version 4) [23] within the density functional theory (DFT). The geometries of the $[CoL_2]^{2+}$ and $[FeL_2]^{2+}$ cations were optimized without symmetry restraints using the PBE0 hybrid functional [24] and the def2-TZVP basis set [25]. The structures obtained from the XRD data were used as the initial approximation. The solvation effects were taken into account within the CPCM model implemented in the ORCA program package (version 4) [23]. Acetonitrile was chosen as the solvent, and NMR spectra were recorded in acetonitrile solutions. The *g*-tensor and hyperfine coupling tensors for protons were calculated on the basis of the obtained geometry for complexes **I** and **II** using the PBE0 hybrid functional [24] and the def2-TZVP [25] basis set with added Gaussian primitives with a high degree of exponent for a more accurate description of the electron density in the core region.

RESULTS AND DISCUSSION

Complexes **I** and **II** were synthesized in high yields by the direct reactions in acetonitrile at room temperature. Since both complexes are poorly soluble in acetonitrile and in the most part of other solvents, they precipitate during synthesis. Complexes **I** and **II** were isolated in the individual form and characterized by elemental analysis and NMR spectroscopy. Their structures were confirmed by the XRD data at 120 K.

Complex **I** (Fig. 1a) crystallizes as a solvate with acetonitrile, diethyl ether, and water, whose molecules are presumably captured from air during the crystallization of the complex from an acetonitrile–diethyl

Table 2. Selected geometric parameters of crystalline complexes **I**, **IIa**, and **IIb***

Complex	Bond	*d*, Å	Angle	ω, deg
I	Co–N(Py)	2.079(3)	θ	84.5(3)
	Co–N(Pz)	2.121(3)–2.167(3)	N(1)CoN(1)	173.16(12)
IIa	Fe–N(Py)	2.1532(14)	θ	85.9(2)
	Fe–N(Pz)	2.1831(15)–2.1955(14)	N(1)FeN(1)	176.56(8)
IIb	Fe–N(Py)	2.136(3)	θ	83.3(4)
	Fe–N(Pz)	2.154(3)–2.199(3)	N(1)FeN(1)	169.60(13)

* θ is the dihedral angle between the root-mean-square planes of the 2,6-di(pyrazol-3-yl)pyridine ligands, and the N(Py) and N(Pz) atoms correspond to the nitrogen atoms of the pyridine and pyrazolyl moieties.

ether mixture. In the crystal the solvent molecules are retained due to hydrogen bonds with the NH and NH_2 groups of the $[CoL_2]^{2+}$ cation (N···O 2.820(4)–3.205(7) Å, NHO 136°–167°; N···N 2.871(7) Å, NHN 152°). The cations form hydrogen bonds with the perchlorate anions (N···O 3.018(8)–3.449(10) Å, NHO 126°–173°), which are bound, in turn, to the solvate water molecule (O···O 2.755(11)–3.169(6) Å, OHO 127°–166°). Under the same conditions, the crystallization of complex **II** gave a mechanical mixture of two types of crystals: solvatomorphs IIa and IIb (Figs. 1b and 1c) that differ in the nature and ratio of solvate molecules ($FeL_2(ClO_4)_2 \cdot 2(C_2H_5)_2O \cdot H_3CN$ (**IIa**) and $FeL_2(ClO_4)_2 \cdot (C_2H_5)_2O \cdot CH_3CN \cdot 0.75H_2O$ (**IIb**)) from each other and from the earlier characterized crystalline solvate **II** with diethyl ether and nitromethane $FeL_2(ClO_4)_2 \cdot 2(C_2H_5)_2O \cdot CH_3NO_2$ [18]. Solvatomorph **IIa** contains one acetonitrile molecule and two molecules of diethyl ether per formula unit of the complex. Solvatomorph **IIb** is the solvate with acetonitrile, diethyl ether, and water in a ratio of 1 : 1 : 0.75. The diethyl ether molecules in solvatomorph **IIa** are retained in the crystal by hydrogen bonds with two NH groups of the $[FeL_2]^{2+}$ cation (N···O 2.729(2) Å, NHO 168(1)°), whereas other NH and NH_2 groups are linked to the perchlorate anions (N···O 2.898(2)–3.190(2) Å, NHO 146°–171°). Solvatomorph **IIb** contains solvent molecules of all the three types (diethyl ether, acetonitrile, and water), which are involved in the hydrogen bonds with one NH_2 group and two NH groups of the $[FeL_2]^{2+}$ cation (N···O 2.845(4)–2.879(8) Å, NHO 154°–167°; N···N 2.966(9) Å, NHN 147°), and the perchlorate anions are bound to the remained NH and NH_2 groups of the cation (N···O 2.905(6)–3.407(9) Å, NHO 130°–171°). The water molecule also forms hydrogen bonds with the acetonitrile molecule and one of the perchlorate anions acting as a proton donor (O···N 2.837(14) Å, OHN 143°; O···O 3.244(10) Å, OHO 152°).

The data obtained from the XRD experiment on the solvent molecules present in the crystals of compounds **I**, **IIa**, and **IIb** and on their nature are consistent with the thermogravimetric (TG) results for finely crystalline samples of the corresponding complexes (Fig. 2). For example, a mass loss of ~8% is observed for cobalt complex **I** on heating in the range from 20 to 200°C (Fig. 2a), which corresponds to the removal of the water and acetonitrile molecules. The diethyl ether molecule was presumably removed from the crystals on drying the sample in vacuo. The vigorous decomposition of the complex begins at 220°C and is accompanied, most likely, by the decomposition of ligand L. Complex **I** loses about 30% of the weight in a range of 220–350°C. The crystalline sample of iron complex **II**, being a mixture of two solvatomorphs **IIa** and **IIb** simultaneously obtained during crystallization from an acetonitril–diethyl ether mixture in air, loses ~5% of the weight in a range of 20–150°C (Fig. 2b), which is associated with the removal of the solvent molecules. At 168°C complex **II** decomposes with explosion and crucible decomposition.

According to the XRD data for the single crystals of compounds **I**, **IIa**, and **IIb** at 120 K, the nitrogen atoms of the 2,6-di(pyrazol-3-yl)pyridine ligands are coordinated to the metal ion (coordination number 6): the distances in the ranges 2.079(3)–2.167(3) and 2.136(3)–2.199(3) Å (Table 2) are typical of cobalt(II) and iron(II) ions in the high-spin state (2.0–2.3 Å [6]). In all cases, the coordination polyhedron MN_6 (M = Co, Fe) [26], which is an octahedron for the low-spin iron(II) ion, is also distorted. In particular, the N(1)MN(1)' angle and the dihedral angle θ between the root-mean-square planes of two ligands (equal to 90° and 180° for an ideal octahedron) are in the ranges 83.3(4)°–85.9(2)° and 169.60(13)°–176.56(8)° in the crystals of compounds **I** and **IIa** and **IIb**, respectively. It should be mentioned that similar values are equal to 87.91(1)° and 177.33(6)° for the earlier described crystalline solvate **II** with diethyl ether and nitromethane $FeL_2(ClO_4)_2 \cdot 2(C_2H_5)_2O \cdot CH_3NO_2$ [18].

The distortion of the MN_6 coordination polyhedron observed in the crystals of compounds **I**, **IIa**, and **IIb** can graphically be presented by means of the so-called "continuous symmetry measures" [27] that describe the deviations from the ideal octahedron S(OC-6) and ideal trigonal prism S(TP-6) (Fig. 3).

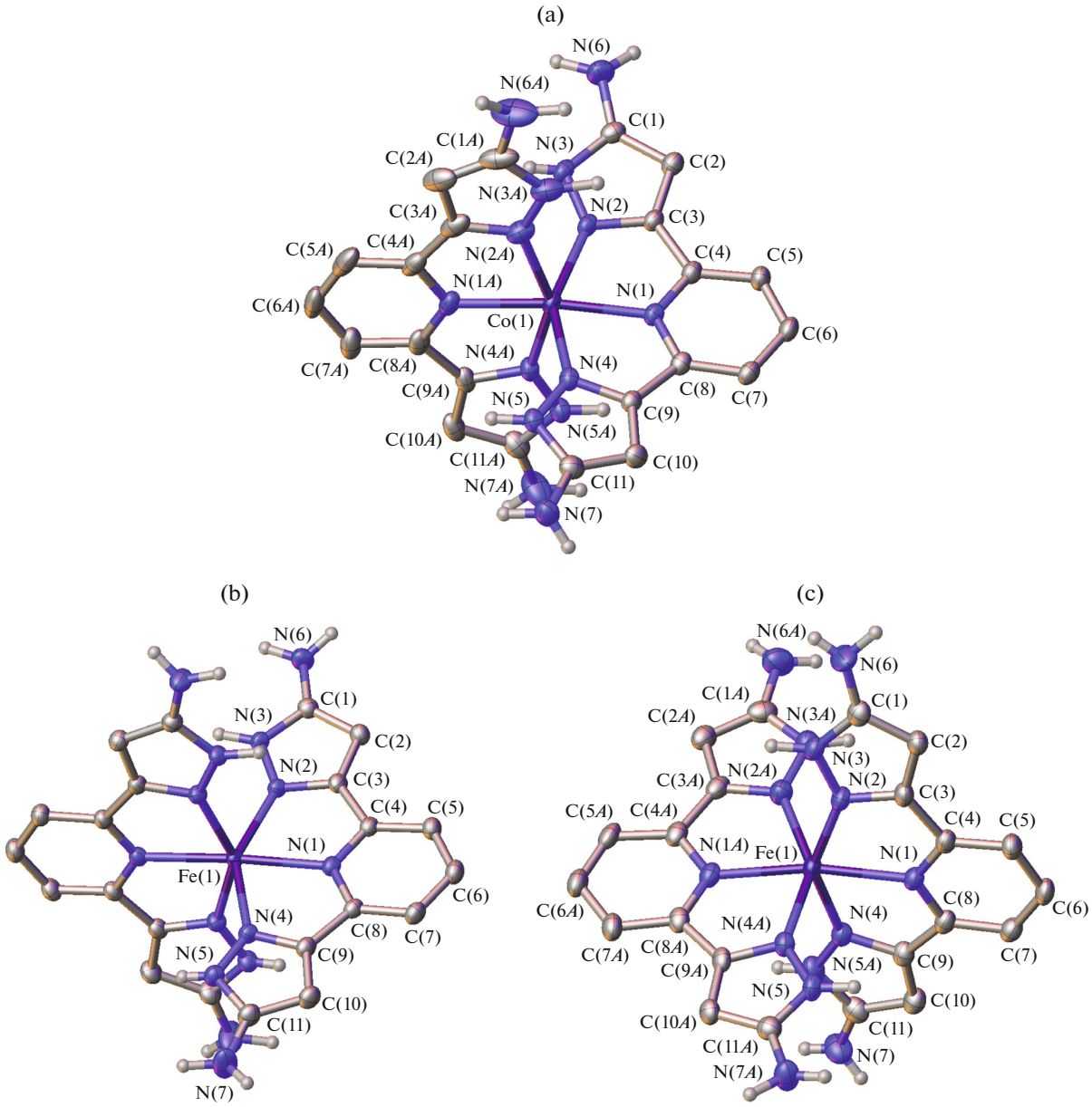

Fig. 1. General view of cations $[ML_2]^{2+}$ (M = Co, Fe) in the crystals of complexes (a) **I**, (b) **IIa**, and (c) **IIb** according to the XRD data in the representation of atoms by thermal ellipsoids (p = 50%). The perchlorate anions, solvent molecules, and hydrogen atoms (except for those belonging to the NH and NH_2 groups) are omitted. In the crystal of complex **IIa** (b), the $[FeL_2]^{2+}$ cation occupies the special position, the 2-fold axis that passes through the iron(II) ion.

The lower these values, the better the description of the shape of the coordination polyhedron (for example, obtained in the XRD experiment) by the corresponding polyhedron. In the case of studied complexes **I** and **II**, the values of the octahedral S(OC-6) and trigonal prismatic S(TP-6) "continuous symmetry measures" (Fig. 3) estimated on the basis of the XRD data for complexes **I** and **IIa** and **IIb** are 9.063–9.377 and 4.665–5.661, respectively, indicating a noticeable distortion of the MN_6 coordination polyhedron toward a trigonal prism. These values also fall in the range of "continuous symmetry measures" S(OC-6) and S(TP-6) characteristic of the high-spin iron(II) complexes with the isomeric 2,6-di(pyrazol-1-yl)pyridine ligands [17].

Thus, the obtained XRD data unambiguously show that the cobalt(II) and iron(II) ions in complexes **I** and **II** exist in the high-spin state at 120 K, and no spin transition is observed in the crystal.

The high-spin state of these complexes in solutions at room temperature was also confirmed by the data of

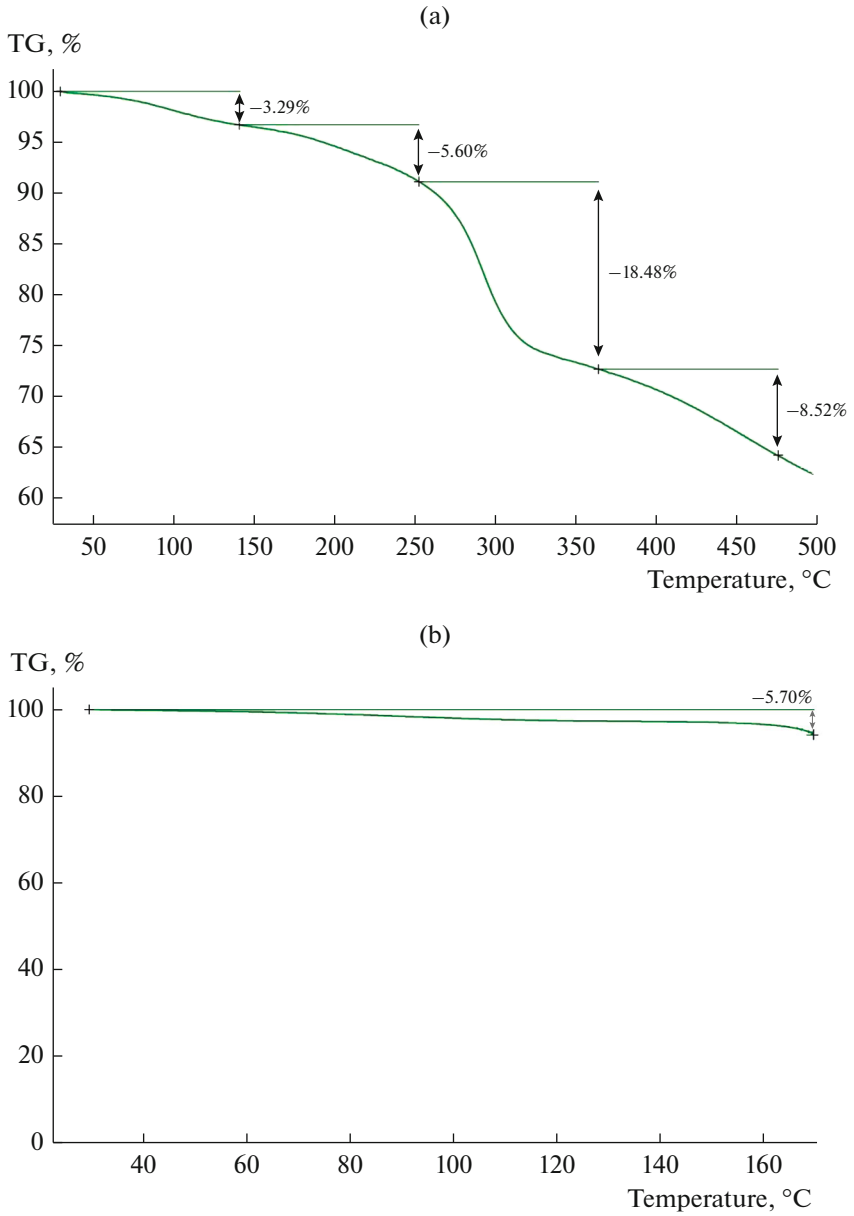

Fig. 2. TG curves for complexes (a) **I** and (b) **II**.

NMR spectroscopy. In particular, the signals in the ^{1}H NMR spectrum for complex **II** (Fig. 4) are far beyond the diamagnetic range (0–15 ppm), which unambiguously indicates the high-spin (HS) state of the iron(II) ion ($S_{HS} = 2$), because its low-spin (LS) state is diamagnetic. Both spin states of the cobalt(II) ion are paramagnetic ($S_{LS} = 1/2$, $S_{HS} = 3/2$). However, in the first case, the values of chemical shifts occur, as a rule, near the diamagnetic region. In the second case, they reach several tens of ppm. Thus, the ^{1}H NMR spectrum obtained for compound **I** (Fig. 4) corresponds to the high-spin cobalt(II) complex.

The earlier proposed original approach to analysis of paramagnetic shifts was used for a more reliable interpretation of the ^{1}H NMR spectroscopic data on the spin states of two complexes in solution [28, 29]. The approach is based on the fact that the nuclei of the complex have very different chemical shifts depending on the spin state of the metal ion. The values of chemical shifts are divided into three components: diamagnetic, contact, and pseudocontact.

$$\delta = \delta_{dia} + \delta_{con} + \delta_{pc}, \quad (1)$$

where δ_{dia} is the diamagnetic contribution, δ_{con} is contact contribution, and δ_{pc} is the pseudocontact contribution.

The δ_{dia} contribution is caused by shielding of the nuclei by the orbital motion of paired electrons, and

the corresponding value of chemical shift in the NMR spectrum for the diamagnetic analog, for example, the isostructural complex of the diamagnetic metal or even the initial ligand, can be accepted to be δ_{dia}. The δ_{con} contribution is determined by the spin density redistribution over the nuclei and is directly proportional to the spin density as follows:

$$\delta_{con} = \frac{4\pi\mu_B^2}{9kT} g^{iso}\rho, \quad (2)$$

where g^{iso} is the isotropic value of g-tensor, and ρ is the spin density. Since it is difficult to obtain the spin density distribution experimentally, it is calculated, as a rule, by quantum chemical methods. In particular, as shown in practice, DFT calculations in combination with hybrid functionals (PBE0, B3LYP, and others) make it possible to estimate the contact contribution for the 3*d*-metal complexes with a fairly high accuracy [28, 30]. The δ_{pc} contribution to chemical shifts appears due to the dipole-dipole interaction of magnetic moments of the nuclei and unpaired electron and, as a consequence, depends on the arrangement of the nuclei relative to the paramagnetic center (metal ion).

$$\delta_{pc} = \frac{1}{12\pi r^3} \times \left[\Delta\chi_{ax}(3\cos^2\theta - 1) + \frac{3}{2}\Delta\chi_{rh}\sin^2\theta\cos 2\varphi\right], \quad (3)$$

where r, θ, and φ are the spherical coordinates of the nuclei in the molecular system of coordinates, and $\Delta\chi_{ax,\ rh}$ are the axial and rhombic anisotropy of the magnetic susceptibility tensor. Therefore, NMR spectra can serve as a source of structural information for paramagnetic compounds, which forms a basis for the use of paramagnetic labels in structural biology [31]. In this case, the problem is solved by the approximation of the experimentally measured chemical shifts at the varied anisotropy parameter of the magnetic susceptibility tensor if the nuclei coordinates in the molecule are known (for example, from the XRD data) and the contact contributions are estimated in the quantum chemical calculations.

Since complexes **I** and **II** are characterized by the axial symmetry, the rhombic component $\Delta\chi_{rh}$ in Eq. (3) becomes zero and the equation for the chemical shift takes the following form:

$$\delta = \frac{1}{12\pi r^3} \times \left[\Delta\chi_{ax}(3\cos^2\theta - 1)\right] + \frac{4\pi\mu_B^2}{9kT} g^{iso}\rho + \delta_{dia}. \quad (4)$$

Thus calculated chemical shifts for complexes **I** and **II** taking into account the high-spin state of the cobalt(II) ion ($S_{HS} = 3/2$) and iron(II) ion ($S_{HS} = 2$) used for the estimation of the δ_{con} contributions according to Eq. (2) and the δ_{dia} contribution taken from the ^{1}H NMR spectrum for the 2,6-di(pyrazol-3-yl)pyridine ligand (Scheme 1) were well consistent with the experimental values (Fig. 5). This confirms the assumption about the high-spin state of complexes **I** and **II** based on an analysis of the chemical shifts in the ^{1}H NMR spectra and indicates the "molecular" nature of this effect.

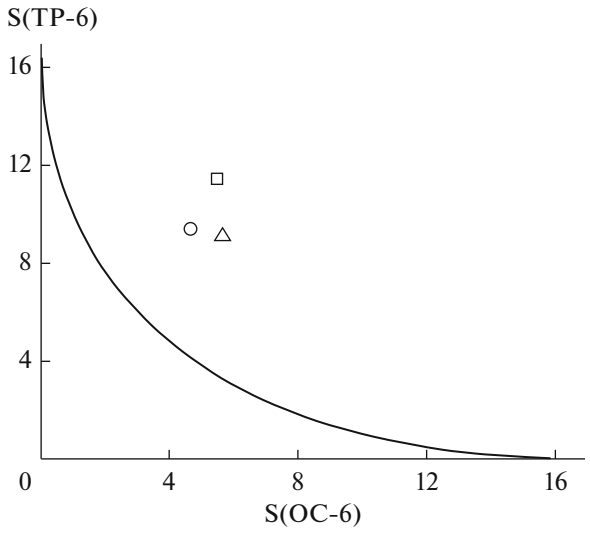

Fig. 3. Graphical representation of deviations of the shape of the MN_6 polyhedron from the ideal trigonal prism TP-6 and ideal octahedron OC-6 by the "continuous symmetry measures" S(TP-6) and S(OC-6) in the crystals of compounds (□) **I**, (○) **IIa**, and (△) **IIb**, respectively. The black line is the minimal distortion pathway between the indicated polyhedra.

To conclude, we synthesized and characterized the cobalt(II) and iron(II) complexes with 2,6-di(5-amino-1*H*-pyrazol-3-yl)pyridine. The XRD data obtained for them (including those for complex **II** in the form of two new solvatomorphs $FeL_2(ClO_4)_2 \cdot 2(C_2H_5)_2O \cdot CH_3CN$ and $FeL_2(ClO_4)_2 \cdot (C_2H_5)_2O \cdot CH_3CN \cdot 0.75(H_2O)$), first of all, the M–N bond lengths and trigonal prismatic distortions of the MN_6 coordination polyhedra unambiguously indicate that the metal ions in the crystal at 120 K exist in the high-spin state ($S = 3/2$ for Co(II) and $S = 2$ for Fe(II)). Both complexes undergo no temperature-induced spin transition at 120–300 K, which was confirmed by the data of ^{1}H NMR spectroscopy at room temperature, including the use of the original approach to an analysis of paramagnetic shifts on the basis of quantum chemical calculations.

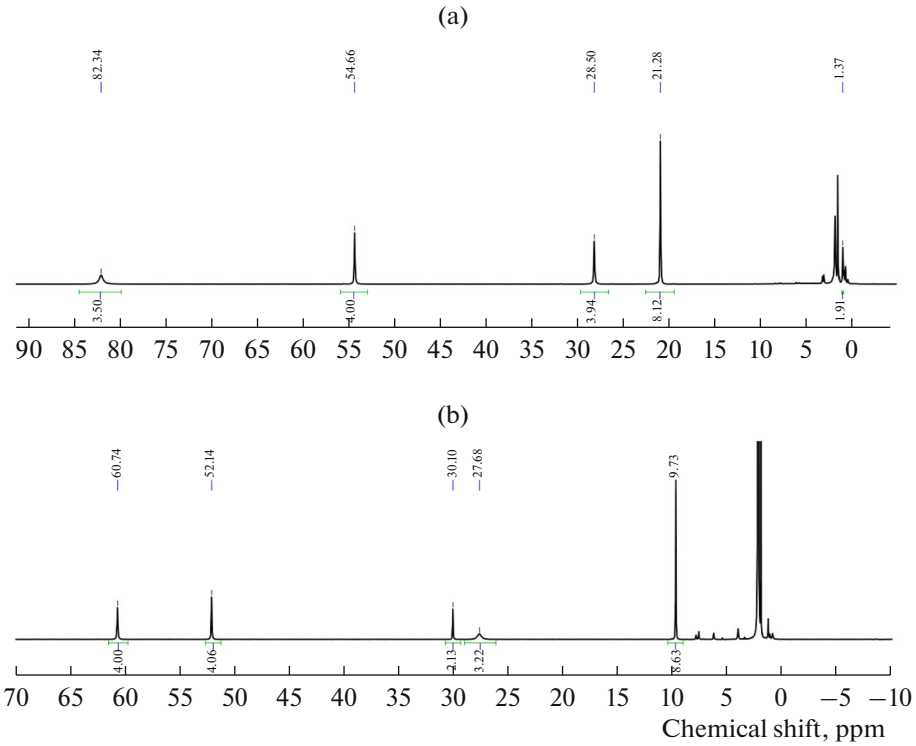

Fig. 4. ^{1}H NMR spectra of complexes (a) **I** and (b) **II** in acetonitrile-d_3 (20°C).

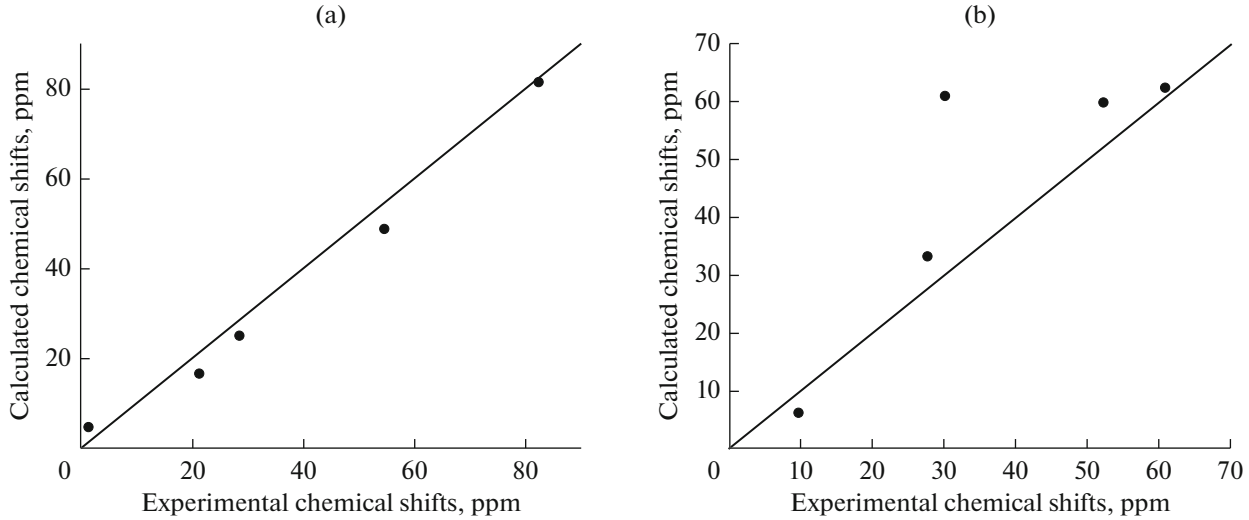

Fig. 5. Comparison of the experimental and calculated chemical shifts in the ^{1}H NMR spectra for complexes (a) **I** and (b) **II** in acetonitrile-d_3 at room temperature.

ACKNOWLEDGMENTS

The structures of the synthesized compounds were studied using the equipment of the Center for Molecular Composition Studies at the Nesmeyanov Institute of Organoelement Compounds (Russian Academy of Sciences).

FUNDING

This work was supported by the Russian Science Foundation, project no. 17-13-01456). A.V. Polezhaev acknowledges the Russian Foundation for Basic Research (project no. 18-33-00561) for the support of thermogravimetric measurements of the synthesized compounds.

REFERENCES

1. Garcia, Y., *Spin Crossover in Transition Metal Compounds I*, Springer, 2004, p. 229.
2. Ferrando-Soria, J., Vallejo, J., Castellano, M., et al., *Coord. Chem. Rev.*, 2017, vol. 339, p. 17.
3. Hayami, S., Holmes, S.M., and Halcrow, M.A., *J. Mater. Chem.*, 2015, vol. 3, no. 30, p. 7775.
4. Molnár, G., Rat, S., Salmon, L., et al., *Adv. Mater.*, 2017, vol. 30, no. 5, p. 1703862.
5. Kumar, K.S. and Ruben, M., *Coord. Chem. Rev.*, 2017, vol. 346, p. 176.
6. *Spin-Crossover Materials: Properties and Applications*, Halcrow, M.A., Ed., Wiley, 2013.
7. Gütlich, P., Gaspar, A.B., and Garcia, Y., *Beilstein J. Org. Chem.*, 2013, vol. 9, p. 342.
8. Judge, J.S. and Baker, W., *Inorg. Chim. Acta*, 1967, vol. 1, p. 68.
9. Harris, C.M., Lockyer, T.N., Martin, R.L., et al., *Aust. J. Chem.*, 1969, vol. 22, no. 10, p. 2105.
10. Novikov, V.V., Ananyev, I.V., Pavlov, A.A., et al., *J. Phys. Chem. Lett.*, 2014, vol. 5, no. 3, p. 496.
11. Bartual-Murgui, C., Codina, C., Roubeau, O., and Guillem, A., *Chem.-Eur. J.*, 2016, vol. 22, no. 36, p. 12767.
12. Hathcock, D.J., Stone, K., Madden, J., and Slattery, S.J., *Inorg. Chim. Acta*, 1998, vol. 282, no. 2, p. 131.
13. Constable, E.C., Housecroft, C.E., Kulke, T., et al., *Dalton Trans.*, 2001, no. 19, p. 2864.
14. Halcrow, M.A., *Coord. Chem. Rev.*, 2005, vol. 249, no. 25, p. 2880.
15. Halcrow, M.A., *Coord. Chem. Rev.*, 2009, vol. 253, no. 21, p. 2493.
16. Kershaw Cook, L.J., Kulmaczewski, R., Mohammed, R., et al., *Angew. Chem., Int. Ed. Engl.*, 2016, vol. 55, no. 13, p. 4327.
17. Kershaw Cook, L.J., Mohammed, R., Sherborne, G., et al., *Coord. Chem. Rev.*, 2015, vols. 289–290, p. 2.
18. Roberts, T.D., Little, M.A., Kershaw, L.J., and Halcrow, M.A., *Dalton Trans.*, 2014, vol. 43, p. 7577.
19. Hynes, M.J. and O'Shea, M.T., *Dalton Trans.*, 1983, no. 2, p. 331.
20. Cook, B.J., Polezhaev, A.V., Chen, C.-H., et al., *Eur. J. Inorg. Chem.*, 2017, vol. 2017, no. 34, p. 3999.
21. Polezhaev, A.V., Chen, C.-H., Kinne, A.S., et al., *Inorg. Chem.*, 2017, vol. 56, no. 16, p. 9505.
22. Sheldrick, G.M., *Acta Crystallogr., Sect. A: Found. Crystallogr.*, 2008, vol. 64, no. 1, p. 112.
23. Neese, F., *Wiley Interdiscipl. Rev. Comput. Mol. Sci.*, 2012, vol. 2, no. 1, p. 73.
24. Adamo, C. and Barone, V., *J. Chem. Phys.*, 1999, vol. 110, p. 6158.
25. Weigend, F. and Ahlrichs, R., *Phys. Chem. Chem. Phys.*, 2005, vol. 7, no. 18, p. 3297.
26. Alvarez, S., *J. Am. Chem. Soc.*, 2003, vol. 125, no. 22, p. 6795.
27. Alvarez, S., *Chem. Rev.*, 2015, vol. 115, p. 13447.
28. Pavlov, A.A., Denisov, G.L., Kiskin, M.A., et al., *Inorg. Chem.*, 2017, vol. 56, no. 24, p. 14759.
29. Pavlov, A.A., Belov, A.S., Savkin, S.A., et al., *Russ. J. Coord. Chem.*, 2018, vol. 44, no. 8, p. 489. https://doi.org/10.1134/S1070328418080067
30. Novikov, V.V., Pavlov, A.A., Nelyubina, Yu.V., et al., *J. Am. Chem. Soc.*, 2015, vol. 137, no. 31, p. 9792.
31. Bertini, I., Luchinat, C., Parigi, G., and Ravera, E., *NMR of Paramagnetic Molecules: Applications to Metallobiomolecules and Models*, Elsevier, 2016, vol. 2.

Translated by E. Yablonskaya